# An improved analytic solution for analysis of particle trajectories in fibrous, two-dimensional filters

H. Marshall
*Scientific Computation Group, Information Technology Division, The University of Michigan, Ann Arbor, Michigan 48109*

M. Sahraoui and M. Kaviany
*Department of Mechanical Engineering and Applied Mechanics, The University of Michigan, Ann Arbor, Michigan 48109*

(Received 2 August 1993; accepted 22 October 1993)

The Kuwabara solution for creeping fluid flow through periodic arrangement of cylinders is widely used in analytic and numerical studies of fibrous filters. Numerical solutions have shown that the Kuwabara solution has systematic errors, and when used for the particle trajectories in filters it results in some error in the predicted filter efficiency. The numerical solutions, although accurate, preclude further analytic treatments, and are not as compact and convenient to use as the Kuwabara solution. By reexamining the outer boundary conditions of the Kuwabara solution, a correction term to the Kuwabara solution has been derived to obtain an extended solution that is more accurate and improves prediction of the filter efficiency. By comparison with the numerical solutions, it is shown that the Kuwabara solution is the high porosity asymptote, and that the extended solution has an improved porosity dependence. A rectification is explained that can make particle collection less efficient for periodic, in-line arrangements of fibers with particle diffusion or body force. This rectification also results in the alignment of particles with inertia (i.e., high Stokes number particles).

## I. INTRODUCTION

Studies of fibrous filters commonly use the idealization of the creeping fluid flow through a periodic arrangement of cylinders, as shown in Fig. 1(a). The assumption of periodicity allows for the analysis of a single fiber with the appropriate boundary conditions. There is no exact analytic, closed-form compact solution for this two-dimensional flow. The Kuwabara[1] creeping fluid flow solution uses a cylindrical unit cell to approximate the local flow through arrangements of cylinders. When used in periodic arrangements of cylinders such as an in-line and isotropic arrangement, the Kuwabara approximation to the square unit cells leads to errors, because the Kuwabara solution does not satisfy the periodic boundary conditions.

The Kuwabara solution is widely used for studies of flow through fibrous filters (e.g., Banks,[2] Banks and Kurowski,[3] and Choo and Tien[4]). Despite this shortcoming with the periodic boundary conditions, many useful results have been derived from the application of this solution to particle capturing in fibrous filters. The Kuwabara solution is compact and can be calculated with only a few operations, which is important, for example, in the Monte Carlo simulations, which require repeated calculations. As will be shown, the Kuwabara solution is also valid as a high porosity asymptote.

Accurate numerical solutions of the flow through equally spaced (i.e., isotropic), periodic arrangement of cylinders has been given by Sangani and Acrivos.[5] Even though their method can be used to obtain high accuracy, there are still some advantages in having an analytic solution, as evidenced by the continued use of the Kuwabara solution. The Kuwabara solution is widely used because it is simple and allows for analytic treatment of the particle capture. However, as mentioned above, it assumes a circular unit cell, and therefore lacks the accuracy in simulating the flow field in a square unit cell. Here improvement to the Kuwabara solution is sought by using an extension that will improve the solution for the square unit cell. This extension of the Kuwabara solution uses a geometric perturbation in order to obtain the square unit cell from the circular unit cell. In order to access the accuracy of this approach, this extended analytic solution is compared with the numerical solutions of the fluid flow through the in-line arrangement of fibers shown in Fig. 1(a). Then this improved analytic solution, the Kuwabara and the numerical solutions, are used to calculate the particle trajectories and the particle capture efficiency. The capture mechanisms considered here are impaction and sieving. Capture by impaction occurs when the particle touches the fiber, and then it is assumed that the particle adheres to the surface. Capture by sieving occurs when the particle diameter is larger than the clearance between the fibers. Hence sieving is geometrical and occurs only in the entrance region of the filter.

In Sec. II we introduce the numerical solution for isotropic and anisotropic, in-line arrangements of cylinders. In Sec. III the analytic correction terms are derived. In Sec. IV the local velocity, the streamfunction solutions and the errors are examined. In Sec. V we show the comparisons of the impaction efficiencies. In Sec. VI we evaluate the derived and the numerical inertial collection efficiencies. In Sec. VII we examine particle rectification effects found in this study.

 1070-6631/94/6(2)/507/14/$6.00  

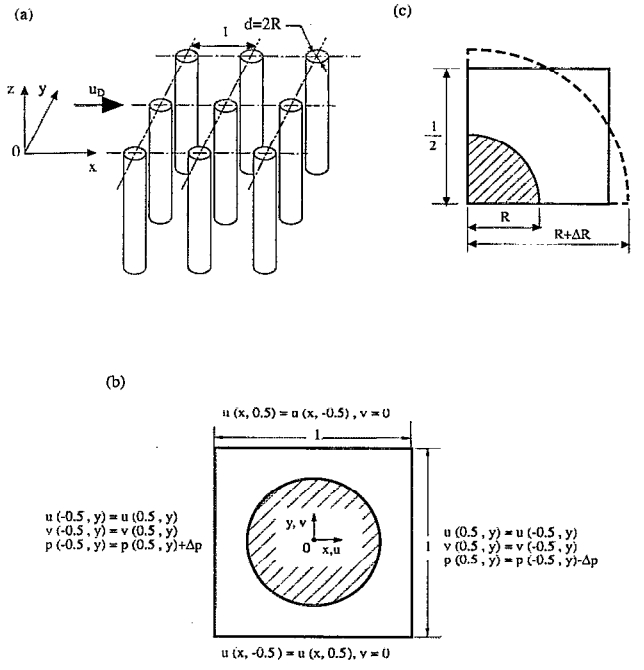


FIG. 1. (a) Periodic arrangement of cylinders with a square unit cell. (b) Boundary conditions used for the numerical solution. (c) Solution domain for the analytic solutions.

## II. NUMERICAL SOLUTION

Sahraoui and Kaviany[6] solved the Navier–Stokes equation for the fluid flow in in-line and staggered arrangements of cylinders. Here the same numerical method is used to solve for the Stokesian flow through an in-line arrangement of fibers. The periodic arrangement of fibers can be represented by the unit cell shown in Fig. 1(b). Due to the presence of the fiber within the square unit cell, the Cartesian coordinates are not accurate for mapping the fiber, unless a very large number of grid points is used. Accurate results can be obtained by using a domain decomposition, where a cylindrical grid net is used near the fiber and a Cartesian grid net is used away from the fiber. Iteration for the solution is performed in both grid nets and a bilinear interpolation is used to communicate between them. In the case where multiple fibers are used, the same procedure is repeated for every fiber. More details about the domain decomposition can be found in Sahraoui and Kaviany[6] and Prata and Sparrow.[7] The equations are nondimensionalized using the length scale $\ell$, the linear dimension of an isotropic unit cell. For anisotropic unit cells, we use the length scale $\ell = \sqrt{\ell_x \ell_y}$ where $\ell_x$ and $\ell_y$ are the dimensions of the unit cell in the $x$ and $y$ directions, respectively. The volume-averaged, $x$ component of the velocity (or Darcean velocity) is used as the velocity scale, and is given by

$$u_D = \langle u \rangle = \int_{-0.5}^{0.5} u \, dy. \tag{1}$$

The governing equations for the fluid flow in the Cartesian coordinates are

$$\frac{\partial u}{\partial x} + \frac{\partial v}{\partial y} = 0, \tag{2}$$

$$-\frac{\partial p}{\partial x} + \frac{\partial^2 u}{\partial x^2} + \frac{\partial^2 u}{\partial y^2} = 0, \tag{3}$$

$$-\frac{\partial p}{\partial y} + \frac{\partial^2 v}{\partial x^2} + \frac{\partial^2 v}{\partial y^2} = 0, \tag{4}$$

and in the cylindrical coordinates, the radial and tangential components of velocity ($v_r$ and $v_\theta$) are given by

$$\frac{\partial r v_r}{\partial r} + \frac{\partial v_\theta}{\partial \theta} = 0, \tag{5}$$

$$-\frac{\partial p}{\partial r} + \left[\frac{1}{r}\frac{\partial}{\partial r}\left(r\frac{\partial v_r}{\partial r}\right) + \frac{1}{r}\frac{\partial}{\partial \theta}\left(\frac{1}{r}\frac{\partial v_r}{\partial \theta}\right)\right] + S_r = 0, \tag{6}$$

$$-\frac{1}{r}\frac{\partial p}{\partial \theta} + \left[\frac{1}{r}\frac{\partial}{\partial r}\left(r\frac{\partial v_\theta}{\partial r}\right) + \frac{1}{r}\frac{\partial}{\partial \theta}\left(\frac{1}{r}\frac{\partial v_\theta}{\partial \theta}\right)\right] + S_\theta = 0, \tag{7}$$

where the source terms $S_r$ and $S_\theta$ are

$$S_r = \left\{-2\frac{v_r}{r^2} + \frac{2}{r^2}\frac{\partial v_\theta}{\partial \theta} + \frac{1}{r}\frac{\partial}{\partial r}\left(r\frac{\partial v_r}{\partial r}\right) + \frac{\partial}{\partial \theta}\left[\frac{\partial}{\partial r}\left(\frac{v_\theta}{r}\right)\right]\right\}, \tag{8}$$

$$S_\theta = \left(-\frac{v_\theta}{r^2} + \frac{2}{r^2}\frac{\partial v_r}{\partial \theta}\right). \tag{9}$$

The above equations are solved by using the no-slip boundary condition on the surface of the fiber and the periodic boundary conditions at the boundaries of the unit cell, as shown in Fig. 1(b).

The momentum equations are solved using the finite-volume method and the pressure correction method, as suggested by Patankar.[8] As will be shown, for low porosities the numerical solutions are more accurate than the Kuwabara solution for the fluid flow in periodic arrangements of cylinders. The numerical integration also allows examination of the flow field in the entrance region of the filter (e.g., Kaviany[9]). In this region the condition of periodicity is not valid. For the study of the particle capture this entrance effect can be important. In Sec. VI E we examine the results of the numerical simulations of the flow in the entrance region for the in-line arrangement of cylinders. For these entrance simulations, we use three fibers aligned in the direction of the flow (i.e., the $x$ direction). Since the fluid flow is not periodic at the inlet, then different boundary conditions are used. At the inlet (i.e., $x=0$), we use

$$u=1, \quad v=0, \quad x=0. \tag{10}$$

At the exit (i.e., $x=L$), we use the periodic boundary condition

$$u(L,y)=u(L-1,y), \quad v(L,y)=v(L-1,y), \quad x=L. \tag{11}$$

### A. Two-dimensional anisotropy

In modeling the flow through fibrous filters, the in-line arrangements of cylinders are usually used. In these models, the periodic unit cell is chosen to have the same length

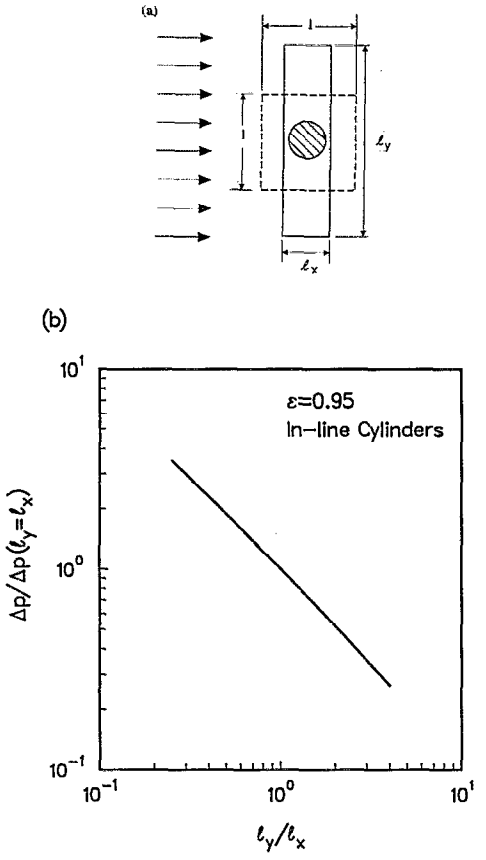


FIG. 2. (a) Unit cell used to examine the effect of cell anisotropy on the pressure drop. (b) Pressure drop for creeping flow over an anisotropic, in-line arrangement of cylinders. The pressure drop is normalized with the isotropic arrangement.

in the longitudinal (along the flow) and the transverse (orthogonal to the flow) directions (i.e., $\ell_x=\ell_y=1$). However, examination of the micrographs of fibrous filters shows that the fibers are very close in the longitudinal direction and far apart in the transverse direction. This anisotropy, among other geometrical factors, contributes to the discrepancy between the predicted and the experimental results for the pressure drop in fibrous filters. Using the two-dimensional numerical simulation, we examine the effect of this anisotropy on the pressure drop by varying the cell dimensions in the $x$ and $y$ directions, as shown in Fig. 2(a). The same porosity and the average flow rate are maintained the same and the pressure drop over the same distance, which is the dimension of the isotropic cell ($\sqrt{\ell_x\ell_y}=1$), is determined. The results of these computations are given in Fig. 2(b), and they show that as the transverse period ($\ell_y$) increases, the pressure drop across the same distance $\ell$ decreases significantly. This result is consistent with the experimental results, which give a pressure drop that is lower by about 60% than that for the square (i.e., isotropic) unit cells (as reported by Liu and Rubow[10]). For $\ell_y/\ell_x=4$ ($\ell_y=2$ and $\ell_x=0.5$), the pressure drop is about 25% of the pressure drop for the isotropic structure. This shows that a significant portion of the pressure drop is due to flow restriction between the cylinders. This is also shown by decreasing $\ell_y$, which results in a significant pressure drop, as shown in Fig. 2(b).

## III. ANALYTIC SOLUTIONS

First, in Sec. III A the Kuwabara solution for the Stokesian flow in a cylindrical domain, as shown in Fig. 1(c), is reviewed. Then, in Sec. III B the extension to this solution for the square unit cell, also shown in Fig. 1(c), is developed. In Sec. III C, the extension to the anisotropic, periodic arrangements is developed.

### A. Kuwabara solution

As mentioned above, the Kuwabara solution[1] approximates the periodic structure by using a cylindrical outer boundary. The governing equation for the streamfunction $\psi$ is given by

$$\nabla^4\psi=0. \tag{12}$$

The boundary conditions at the surface of the fiber are

$$v_r=v_\theta=0, \quad \text{at } r=R, \tag{13}$$

where $v_r$ and $v_\theta$ are given by

$$v_r=\frac{1}{r}\frac{\partial\psi}{\partial\theta} \quad \text{and} \quad v_\theta=-\frac{\partial\psi}{\partial r}. \tag{14}$$

For the outer boundary, Kuwabara uses

$$v_r=\cos\theta \quad \text{and} \quad \omega=0, \quad \text{at } r=R+\Delta R, \tag{15}$$

where $\omega$ is the vorticity. The solution to Eq. (12) is

$$\psi(r,\theta)=R\left[C_1\left(\frac{r}{R}\right)^3+C_2\frac{r}{R}+C_3\frac{R}{r}+C_4\frac{r}{R}\ln\left(\frac{r}{R}\right)\right]\sin\theta. \tag{16}$$

The coefficients $C_1$ to $C_4$ are found using the boundary conditions (13)–(15), and they are given by

$$C_4=-\frac{4}{2\ln(1-\epsilon)-1+4\epsilon+(1-\epsilon)^2}, \tag{17}$$

$$C_1=-\frac{(1-\epsilon)C_4}{4}, \tag{18}$$

$$C_3=C_1+\frac{C_4}{2}, \tag{19}$$

$$C_2=-C_1-C_3, \tag{20}$$

where $\epsilon$ is the porosity given by

$$\epsilon=1-\pi R^2, \tag{21}$$

and for the circular unit cell it is given by

$$\epsilon=1-\left(\frac{R}{R+\Delta R}\right)^2. \tag{22}$$

### B. Extended analytic solution

The purpose of extending or improving the Kuwabara solution are threefold. It is practical to find a new solution

that is more accurate, but still compact and not of overwhelming complexity nor a slowly converging series, such as the one suggested by Hasimoto.[11]

Since the Kuwabara solution is in much use, and as we shall show later, in the limit of high porosity it is a good approximation, the new analytic solution is obtained by adding a correction term to the Kuwabara solution. This additive correction form is possible because of the linear superposition of the eigenfunctions of the biharmonic operator.

From the boundary conditions for the Kuwabara solution in Eq. (15), we note that the only element of a periodic cell or even a square surrounding cell is that the outer radius can be chosen so that the solid fraction of this cylindrical region is the same as the square unit cell. This is indeed how the Kuwabara solution is used (e.g., Banks[2]). No other influence of the square unit cell is found in the Kuwabara solution. This greatly reduces the mathematical complexity since the eigenfunctions of the equations have a convenient form in the cylindrical coordinates, but reduces the accuracy of the solution away from the cylinder, which, in turn, affects the accuracy of the prediction of the particle trajectories and collections.

In this extended analytic solution we attempt to correct for this problem. Due to the symmetry of the geometry and the flow considered, we can fold the domain into one-quarter, as shown in Fig. 1(c). The boundary conditions we use along the cylinder surface are the same as the no-slip boundary in the Kuwabara solution. These are the appropriate boundary conditions, as long as the mean-free path of fluid molecules is much smaller than the fiber diameter. The equations to be solved for this creeping flow are

$$\nabla^2\psi=\omega, \tag{23}$$

$$\nabla^2\omega=0. \tag{24}$$

The streamfunction solution, which satisfies these governing equations in a square unit cell and the no-slip boundary conditions in the cylindrical coordinates, is known (e.g., Sangani and Acrivos[5]), and is

$$\psi=\left\{a_1r^3\left[1-\frac{4\ln r}{2\ln R+1}\left(\frac{R}{r}\right)^2\frac{2\ln R-1}{2\ln R+1}\left(\frac{R}{r}\right)^4\right]+b_1R^2r\left[1-\frac{2\ln r}{2\ln R+1}-\left(\frac{R}{r}\right)^2\frac{1}{2\ln R+1}\right]\right\},$$

$$\sin\theta+\sum_{n=2}^{N}\left\{a_nr^{2n+1}\left[1-2n\left(\frac{R}{r}\right)^{4n-2}+(2n-1)\left(\frac{R}{r}\right)^{4n}\right]\times b_na^2r^{2n-1}\left[1(2n-1)\left(\frac{R}{r}\right)^{4n-4}+2(n-1)\left(\frac{R}{r}\right)^{4n-2}\right]\right\}\times\sin(2n-1)\theta. \tag{25}$$

Sangani and Acrivos[5] have used the collocation method (a spectral numeric method) to solve for the spectral coefficients $a_n$ and $b_n$. This is done by using the appropriate boundary conditions at some discrete points on the Cartesian boundary of the square unit cell. Then they form linear equations for the coefficients $a_n$ and $b_n$ for each boundary collocation point. This provides an accurate numerical method of solving for the fluid flow.

The outer boundaries of the square unit cell in Fig. 1(c) can be represented, in the cylindrical coordinates, as having a distance $r$ from the center point and an angle $\theta$. Then we can define $\delta(\theta)$ such that when it is added to the outer radius $R+\Delta R$, it gives the square unit cell in the polar coordinates as

$$r=(R+\Delta R)+\delta(\theta). \tag{26}$$

Note that $\delta(\theta)$ for the square geometry is always less than 0.23. Thus $\delta(\theta)$ is always a small parameter and can be considered as a perturbation. This is a perturbation expansion from a cylinder to a square. The expansion of the streamfunction is given by

$$\psi=\psi_0+\delta\psi_1+\delta^2\psi_2. \tag{27}$$

Substituting this into the linear biharmonic, Eq. (12) gives

$$\nabla^4\psi_0=0, \quad \text{at order } \delta^0, \tag{28}$$

$$\nabla^4\psi_1=0, \quad \text{at order } \delta^1. \tag{29}$$

The boundary conditions we will use are

$$\frac{\partial v}{\partial x}=0, \quad \text{at } x=0.5 \tag{30}$$

and

$$\frac{\partial\omega}{\partial x}=0, \quad \text{at } y=0.5. \tag{31}$$

The problem with these boundary conditions is that there is no explicit dependence on $\delta(\theta)$. This can be obtained by a perturbative expansion of the boundary condition and a Taylor expansion about $R+\Delta R$. The result is

$$\frac{\partial v_0}{\partial x}(r,\theta)=\frac{\partial v_0}{\partial x}(r,\theta)\Big|_{R+\Delta R}+\frac{\partial}{\partial r}\frac{\partial v_0}{\partial x}(r,\theta)\Big|_{R+\Delta R}\delta(\theta). \tag{32}$$

The order $\delta^0$ boundary condition is

$$\frac{\partial v_0}{\partial x}(r,\theta)\Big|_{R+\Delta R}=0, \tag{33}$$

and for the $\delta^1$ is

$$\frac{\partial v_1}{\partial x}(r,\theta)\Big|_{R+\Delta R}=\frac{\partial v_0}{\partial x}(r,\theta)\Big|_{R+\Delta R}\delta(\theta). \tag{34}$$

Note the explicit dependence of the boundary condition on the geometry. Then $\delta^1$ can be expanded in a Fourier series in $\sin[(2n-1)\theta]$, and the boundary conditions are used to calculate the coefficients in Eq. (25).

The resulting solution is not very accurate for low truncations. For high truncations the formula becomes excessively large. Sangani and Acrivos[5] used 6–40 terms for accurate numerical solutions. This analytic method will produce accurate results if enough terms are included from the expansions. However, it does not provide a useful, compact formula. For this analytic form, each successive

coefficient depends on the previous coefficients. Thus the length of the analytic solution becomes overwhelming for this method. In contrast, our goal is to obtain a reasonably compact analytic solution.

The problem is that the basic state of the perturbation is not a very efficient approximation. The Kuwabara solution is a better approximation than the lowest term in Eq. (25) with the above approximations. The above solution method is more accurate only when enough expansion terms are included. Since our goal is to have both an accurate and compact formula, the Kuwabara solution is used as our basic state. Note that the streamfunction obtained by Kuwabara is essentially the $\sin\theta$ term in Eq. (25) with a particular choice of the coefficients. Thus our solution is still of the form of Eq. (25). With the Kuwabara solution as the basic state, we proceed with a streamfunction given by

$$\psi=\psi_K+\psi_E, \tag{35}$$

where $\psi_K$ is the streamfunction obtained from the Kuwabara solution and $\psi_E$ is the extension that is that part of Eq. (25) having the higher-order terms of $\sin[2(n-1)\theta]$. As will be shown in the next section, the rectangular periodic cell requires $\sin(2n\theta)$ due to symmetry changes. The error in the streamfunction for the Kuwabara solution in a periodic cell, we hypothesize should have a symmetry similar to the perturbation parameter $\delta$ defined in Eq. (26). The perturbation $\delta$, in turn, has a symmetry like the first term of Eq. (25). The convergence of this approximation will be the test of this hypothesis.

The advantage of this formulation is that the Kuwabara solution is a more efficient choice than the first term of Eq. (25). However, the problem with this formulation is that Kuwabara's boundary conditions are not appropriate to the square unit cell. In order that $\psi$, the total streamfunction, has the correct boundary conditions, we must impose a boundary condition on $\psi$ and then subtract the Kuwabara solution to obtain the boundary condition for $\psi_E$. The two boundary conditions on the total streamfunction we use are

$$\int_0^{1/2} u\,dy=\Delta\psi, \quad \text{at } x=-0.5, \tag{36}$$

$$\int_0^{1/2} v\,dx=0, \quad \text{at } y=0.5. \tag{37}$$

These boundary conditions are chosen to correct for the flow (as predicted by the Kuwabara solution) from the top of one cell to another [Eq. (37)] and to retain the correct mass flow rate through the filter [Eq. (36)]. If both Eqs. (36) and (37) are satisfied the correct outflow is attained as well. More general boundary conditions that include these as a subset can be used. We have used other and more general boundary conditions, and no improvement in predicting the local velocity is achieved. Higher-order terms greatly complicate the analytic formula and reduce the error in the formula by less than a few percent per term. Thus our extended solution only includes one higher-order $\sin\theta$ term than does the Kuwabara solution. However, as we shall show in Sec. IV the above boundary conditions are adequately satisfied for many situations. Other expansion terms need to be included for the anisotropic unit cells, and this will be discussed in Sec. III C.

The resulting extended solution for the total streamfunction is

$$\psi(r,\theta)=R\left[C_1\left(\frac{r}{R}\right)^3+C_2\frac{r}{R}+C_3\frac{R}{r}+C_4\frac{r}{R}\ln\left(\frac{r}{R}\right)\right]\times\sin\theta+\left\{C_5R^2r^3\left[1+2\left(\frac{R}{r}\right)^6-3\left(\frac{R}{r}\right)^4\right]+C_6r^5\left[1+3\left(\frac{R}{r}\right)^8-4\left(\frac{R}{r}\right)^6\right]\right\}\sin(3\theta), \tag{38}$$

where $C_5$ and $C_6$ are given by

$$C_5=-C_7(-8R^2+256R^8-384R^{10})-C_8(-R^2+256R^8-768R^{10}), \tag{39}$$

$$C_6=-C_7(16R^4-192R^8+256R^{10})-C_8(4R^4-192R^8+512R^{10}), \tag{40}$$

where $C_7$ and $C_8$ are given by

$$C_7=\frac{4C_1-16R^2+16C_2R^2+64C_3R^4+16C_4R^2\ln(1/2R)}{C_9}, \tag{41}$$

$$C_8=\frac{16C_1-32R^2+32C_2R^2+64C_3R^4+32C_4R^2\ln(1/\sqrt{2}R)}{C_9}, \tag{42}$$

and $C_9$ is given by

$$C_9=16R^6-1344R^{10}+6912R^{12}-10752R^{14}+8192R^{18}. \tag{43}$$

The coefficients $C_1$ through $C_4$ are the coefficients of the Kuwabara solution and are given by Eqs. (17)–(20). The coefficients of this extended solution depend only on the porosity and the radius of the fiber, and for a set of porosity and radius they are constants. The equations were manipulated using the MATHEMATICA *software* (MATHEMATICA is a Copyright of the Wolfram Research Inc).

Equation (38) is valid for small Reynolds number (i.e., $\mathrm{Re}<1$) and typical filters have Reynolds numbers of 0.1 or less. Porosities from 0.5 to 1 have been tested (Secs. IV and V). However, typical filters are in the range of 0.8–0.95.

### C. Anisotropic extension of Kuwabara solution

Many filters have fibers that are spaced closer together in the flow direction than in the perpendicular direction. To study the effect of this anisotropic distribution of fibers, we have examined anisotropic extension of the Kuwabara solution to an anisotropic array of fibers. More appropriately, this is an extension of the extended solution discussed in the last section. As we will show this anisotropic extension to the Kuwabara solution does improve the ac-

curacy of the solution for fibers spaced unequally in the $x$ and $y$ directions. However, the compactness of the coefficients found in the last section is lost.

The same geometry is used as in Figs. 1(b) and 1(c). However, the periodic rectangular cells have nonequal sides $\ell_x$ and $\ell_y$ with the total area $\ell_x\ell_y=1$. Equation (2.4) from Sangani and Acrivos[5] is no longer valid. It implicitly assumes the distance from the cylinder to the edge of the cell is equal in both $x$ and $y$ directions. We find that one more extended term plus the one we added in the last section are needed to obtain reasonable solutions with at least some degree of compactness.

The method of solution is much the same as in Sec. III B, so we will only point out to the differences. The basic Kuwabara solution is not the most efficient zeroth-order term, but with some small modifications it can be made into a first-order term. We modify the Kuwabara solution by applying the boundary conditions on an ellipse with axes equal to the rectangular axes. We retain the extended term with undetermined coefficients of the last section. Finally, we add a $\sin 2\theta$ term that is the lowest-order term and is not found in Eq. (25) because of the previously assumed symmetry. The same boundary condition is used as in the previous section only the integrals in Eqs. (36) and (37) are divided into smaller segments of the boundaries.

The resulting solution is not as compact as Eq. (38). However, it becomes compact once a porosity and a ratio of $\ell_y$ to $\ell_x$ is chosen. The reason is the dependence of the coefficients on the porosity and the geometry is rather complex. For a porosity of 0.95 and $\ell_y/\ell_x=1.44$, the solution is

$$\psi(r,\theta)=9.362\times10^{-2}\left(\frac{7.714\times10^{-2}}{r}-4.723r-7.809r^3+9.943r\ln(7.927r)\right)\sin\theta+\left[3.132\times10^{-1}\left(1+\frac{8.063\times10^{-6}}{r^6}-\frac{7.600\times10^{-4}}{r^4}\right)r^4-1.203\times10^{-1}\left(1+\frac{2.533\times10^{-4}}{r^4}-\frac{3.183\times10^{-2}}{r^2}\right)r^2\right]\sin2\theta+\left[1.043\times10^{-1}\times\left(1+\frac{1.925\times10^{-7}}{r^8}-\frac{1.613\times10^{-5}}{r^6}\right)r^5-2.252\times10^{-1}\left(1+\frac{8.063\times10^{-6}}{r^6}-\frac{7.600\times10^{-4}}{r^4}\right)r^3\right]\sin3\theta. \quad (44)$$

The same anisotropy and a porosity of 0.80 gives the following expression:

$$\psi(r,\theta)=1.593\times10^{-1}\left(\frac{4.640\times10^{-1}}{r}-6.478r-12.72r^3+16.20r\ln(3.963r)\right)\sin\theta+\left[1.172\left(1+\frac{5.160\times10^{-4}}{r^6}-\frac{1.216\times10^{-2}}{r^4}\right)r^4-5.625\times10^{-1}\left(1+\frac{4.053\times10^{-3}}{r^4}-\frac{1.273\times10^{-1}}{r^2}\right)r^2\right]\sin2\theta+\left[2.374\times10^{-2}\times\left(1+\frac{4.928\times10^{-5}}{r^8}-\frac{1.032\times10^{-3}}{r^6}\right)r^5-4.770\times10^{-1}\left(1+\frac{5.160\times10^{-4}}{r^6}-\frac{1.216\times10^{-2}}{r^4}\right)r^3\right]\sin3\theta. \quad (45)$$

Equations (44) and (45) have been derived for an angle $\theta$ between 0 and $\pi/2$. Using the same formula for angles larger than $\pi/2$ leads to errors. For these angles symmetry is used to calculate the streamfunction.

We have a closed-form analytic solutions for the coefficients of the above equation. These can be provided via e mail (however, the length approximates the length of this article). These solutions can be manipulated via a computer algebra program such as MATHEMATICA or MAPLE.

In Sec. IV we show the results of this solution as we compare them with the numerical results.

## IV. COMPARISON OF VARIOUS SOLUTIONS

As previously discussed, numerical solutions to this problem are known (e.g., the numerical solutions of Sangani and Acrivos[5]), and are more accurate than the analytic solutions. Thus the numerical results from Sec. II will be our standard for the comparison.

The streamfunction contours using the Kuwabara, the extended, and the numerical solutions are shown in Fig. 3. Note that the Kuwabara solution has streamlines crossing the upper boundary of the unit cell in error. As we shall show later this has negative consequences for calculations of the particle collection efficiency. The extended analytic and the numerical solution show that the flow does not cross the upper boundary of the cell, as expected. Figure 3 also shows that the numerical and the extended analytic solution are in good agreement above the fiber. However, at the exit and inlet boundaries, the extended analytic solution deviates from the numerical solution. Further comparisons of the different solutions are given below in terms of the velocity fields.

In Figs. 4(a) and 4(b) we show the velocity errors in both the Kuwabara solution and the extended analytic solution. The velocity error fields for both are constructed by subtracting the velocity fields from that of the numerical solution. Both Figs. 4(a) and 4(b) are scaled similarly. The magnitude of the largest error vector for the Kuwa-

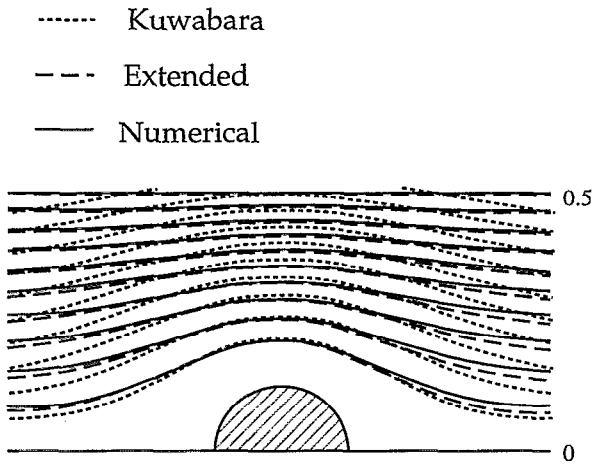


FIG. 3. Constant streamfunction contours for the Kuwabara solution, extended analytic solution, and numerical solution ($\epsilon=0.95$).

bara solution is 0.349, while that of the extended analytic solution is 0.119, and occurs at the inlet and exit boundaries of the unit cell. These results show that the extended analytic solution improves the prediction of the local flow field over the Kuwabara solution, especially near the upper boundary of the cell. This is also shown in Fig. 3, where the streamfunction contours for the extended analytic solution near the upper boundary is almost rectilinear, as expected.

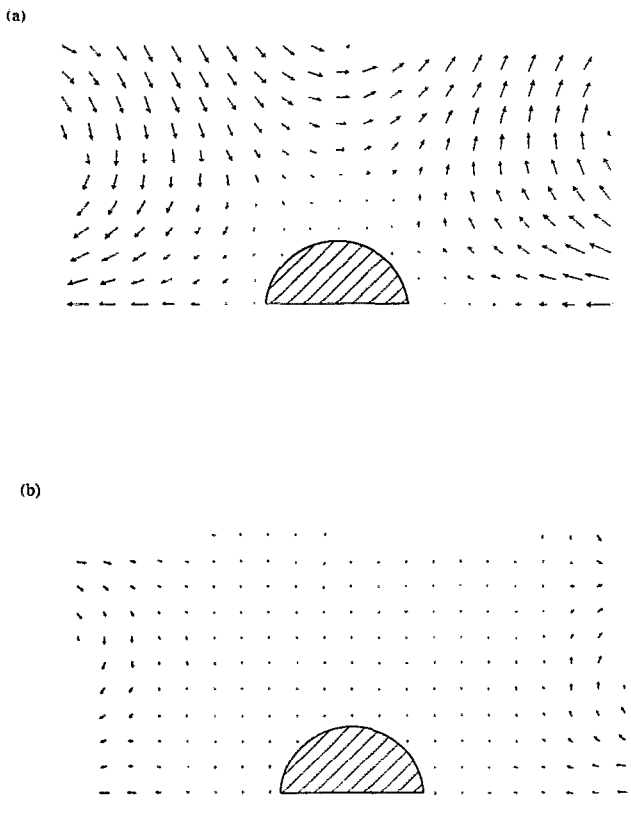


FIG. 4. Comparison of the local velocity vector between the two analytic solutions and the two-dimensional numerical solution (a) extended analytic solution and (b) Kuwabara solution ($\epsilon=0.95$).

TABLE I. Pressure drop predictions for the Kuwabara solution, the extended, and the numerical solutions for the in-line arrangement of cylinders.

| $\epsilon$ | Kuwabara | Extended | Numerical |
|---|---|---|---|
| 0.5 | 368.2 | 344.6 | 533.4 |
| 0.6 | 184.1 | 177.9 | 218.3 |
| 0.7 | 96.88 | 95.25 | 103.2 |
| 0.8 | 49.94 | 49.64 | 50.26 |
| 0.9 | 25.15 | 25.15 | 24.87 |
| 0.95 | 15.74 | 15.76 | 15.57 |

This is an important feature of the analytic solution, since mass flow conservation is satisfied at every cross section of the square unit cell. The Kuwabara solution has a discontinuity in the upper boundary streamfunction when connected to the adjoint cell.

We have also made the same comparisons for $\epsilon=0.8$, and we have found that the discrepancy between the Kuwabara solution and the numerical solution is larger. The magnitude of the maximum error vector is 0.690, which occurs at the inlet and exit boundaries of the unit cell. The maximum error for the extended analytic solution is 0.205.

The various solutions are also compared by evaluating the pressure drop for different porosities. The results are presented in Table I. These results show that for high porosity (i.e., $\epsilon\geqslant 0.8$), excellent agreement between the numerical solution and the analytic solutions is obtained. Note that for fibrous filters the porosity is larger than 0.8. For $\epsilon=0.7$, the difference between the extended analytic solution and the numerical solution is about 7%, which is acceptable. For lower porosity (i.e., $\epsilon\leqslant 0.6$), the accuracy of the analytic solutions in predicting the pressure drop deteriorates further, and a difference of 20% is obtained. Since the extended analytic solution is intended to correct the Kuwabara solution near the outer boundary of the unit cell, the flow near the cylinder is not altered significantly. Thus, the Kuwabara and the extended analytic solutions predict pressure drops that are very close.

In Fig. 5 we show the error for the extended anisotropic solution with $\ell_y/\ell_x=1.44$. The magnitude of the

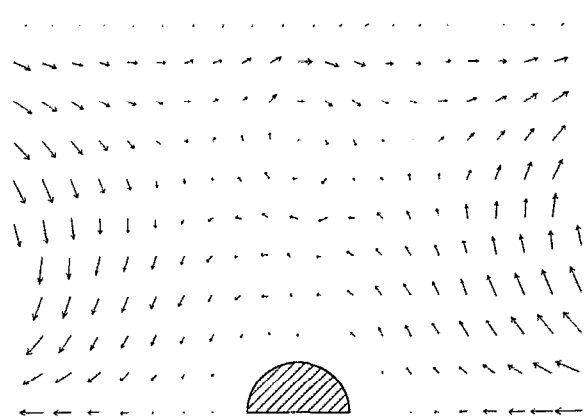

FIG. 5. Comparison of the local velocity vector between the extended analytic solution for the anisotropic unit cell for $\epsilon=0.95$ and $\ell_y/\ell_x=1.44$.

maximum error vector is 0.182, which is slightly larger than that for the square cell. Most of the error in the velocity vector occurs near the exit boundaries of the unit cell. Thus for small stretches in the $y$ direction, the anisotropic analytic solution gives good estimates of the particle collection efficiency (this will be discussed below).

## V. PARTICLES IMPACTION EFFICIENCY

To examine the utility of the extended solution, we begin with the particle impaction and the study of particle capture in filters with negligible diffusion, negligible surface forces, and for particles with negligible inertia. Without the inertial effects, the particle paths are entirely determined by the fluid flow. We assume that particles do not affect the local flow and thus follow the streamlines. The opposite extreme is the case where the particle inertia is so large (i.e., the Stokes number is large), such that there are no fluid flow effects on the particle collection. Particle inertia is explored in the next two sections.

In Fig. 6, the geometry in aspects of the particle impaction are shown. A particle of radius $R_p$ is collected if it impacts the fiber, otherwise it is uncollected. There is a critical streamline that distinguishes between the collected and the uncollected particles for a given $R_p$. For these calculations, we assume that the fluid entering this unit cell has a uniform distribution of particles. The efficiency is simply the ratio of the collected particles to the total particles. For particles larger than the openings between fibers, sieving occurs and then they are all collected.

For each particle radius there is a limiting streamline that separates the flow region where particles are collected from the flow region where the particles are not collected. Thus the streamfunction with $\theta$ set to $\pi/2$ and the radius $r$ replaced by the fiber radius $R$ plus the particle radius $R_p$ in Eq. (38), becomes an analytic relationship for the particle collection, which is the advantage of having an analytic solution for the fluid flow. We can derive a particle collection formula rather than having to recalculate the efficiency for each particle. The particle capture efficiency is given by

$$\eta = 200\psi\left(R_p+R, \frac{\pi}{2}\right) \tag{46}$$

$$= 200R\left[C_1\left(\frac{R_p+R}{R}\right)^3 + C_2\frac{R_p+R}{R} + C_3\frac{R}{R_p+R} + C_4\frac{R_p+R}{R}\ln\left(\frac{R_p+R}{R}\right)\right] - 200\left\{C_5R^2(R_p+R)^3 \times\left[1+2\left(\frac{R}{R_p+R}\right)^6 - 3\left(\frac{R}{R_p+R}\right)^4\right] + C_6(R_p+R)^5 \times\left[1+3\left(\frac{R}{R_p+R}\right)^8 - 4\left(\frac{R_p+R}{r}\right)^6\right]\right\}. \tag{47}$$

Assuming particles do not affect the local flow, the entire range of $R_p/R$ is valid. For small particle ($R_p<R$), the above efficiency expression can be simplified:

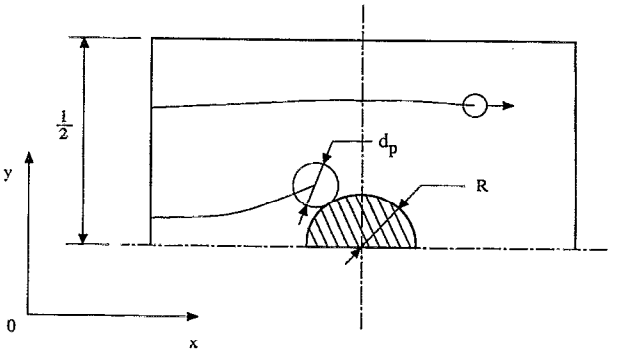


FIG. 6. Impaction schematic.

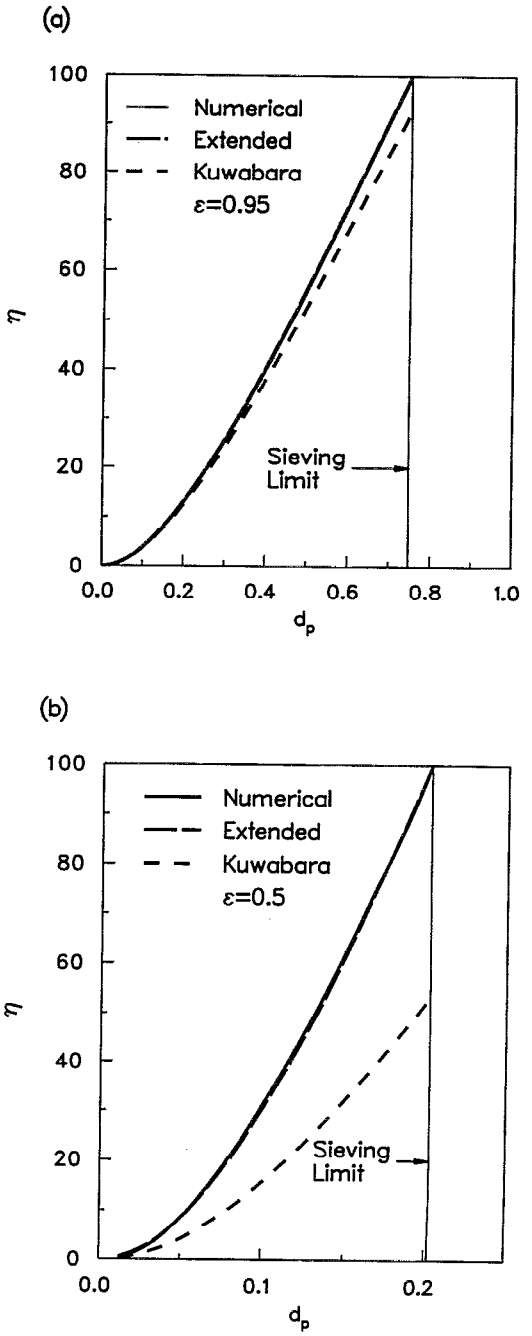


FIG. 7. Particle impaction efficiency for uniformly distributed particles in the flow using (a) $\epsilon=0.95$ and (b) $\epsilon=0.5$.

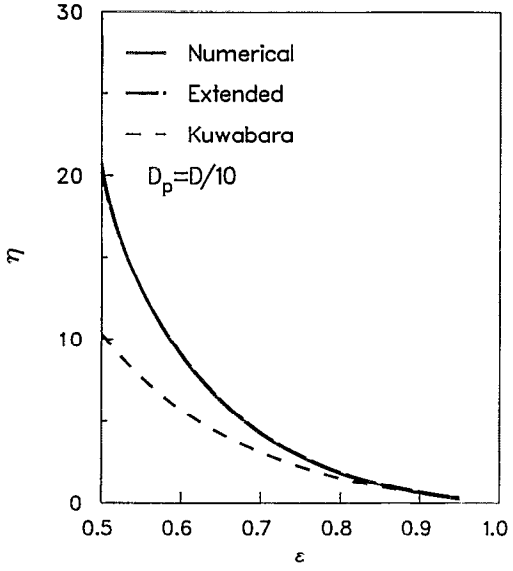


FIG. 8. Collection efficiency error as a function of porosity ($R_p=R/10$).

$$\eta=200R\left[C_1+C_2+C_3+\frac{R_p}{R}(3C_1+C_2-C_3)+C_4\frac{R_p}{R}\left(1+\frac{R_p}{R}\right)\right]-200\left(12C_5\frac{R_p^2}{R^3}+24C_6\frac{R_p^2}{R^7}\right). \tag{48}$$

From Figs. 7(a) and 7(b), one can see that close to the cylinder (i.e., small $d_p$) both the Kuwabara and the extended analytic solution are accurate. The extended analytic solution is also accurate near the edge of the periodic unit cell (i.e., large $R_p=d_p/2$). The particle collection efficiency derived from the extended analytic solution is in excellent agreement with those from the numerical results. The results from the Kuwabara solution are less accurate than the extended analytic solution, especially for lower porosity, as shown in Fig. 7(b). The Kuwabara error increases linearly while increasing the porosity. This is shown in Fig. 8, where the particle collection efficiency for $R_p=R/10$ is shown for a variable porosity. For low porosity the discrepancy between the numerical and the Kuwabara solutions is large, but the extended solution is in good agreement for the entire range of porosity shown.

Figures 9(a) and 9(b) depict the efficiency predicted by the anisotropic extended solution given by Eqs. (44) and (45) and computed in the same manner as above for the square cell, i.e., Eq. (47). The results are for $\ell_y/\ell_x=1.44$. As shown, a good agreement is found with the numerical results for both porosities.

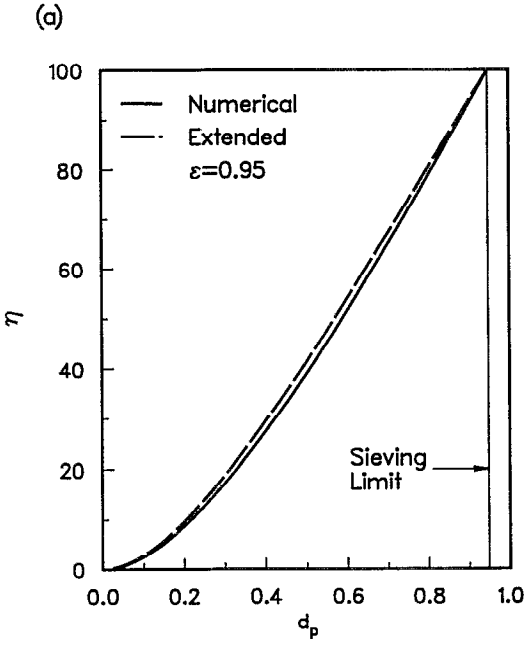


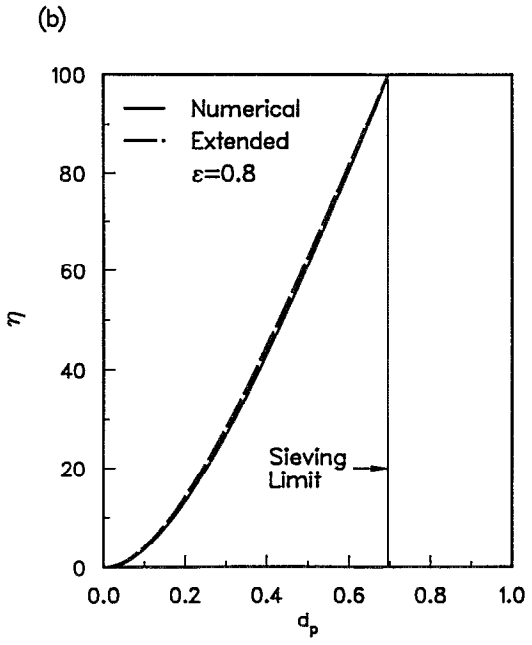


FIG. 9. Particle impaction efficiency for anisotropic unit cells using uniformly distributed particles in the flow (a) $\epsilon=0.95$ and (b) $\epsilon=0.8$ ($\ell_y/\ell_x=1.44$).

## VI. INERTIAL PARTICLE COLLECTION EFFICIENCY

One major mechanism for collection of heavier particles in the absence of external forces is the inertial impaction. In the previous section we ignored the particle inertia. The extent of the particle collection can be determined once the particle trajectories through the fiber lattice is known. The trajectories can be calculated by using the force balance on a particle. The Lagrangian particle momentum equation is given by (Tien[12])

$$c_s\frac{4}{3}\pi R_p^{*3}\rho_p^*\frac{d\mathbf{u}_p^*}{dt^*}=6\pi\mu^*R_p^*(\mathbf{u}^*-\mathbf{u}_p^*), \tag{49}$$

where $R_p^*$ is the radius of the particle, $\mathbf{u}^*$ is the fluid velocity vector, $\mathbf{u}_p^*$ is the particle velocity vector, $\mu^*$ is the dynamic viscosity of the fluid, and $c_s$ is the Cunningham correction factor, which accounts for the velocity slip when

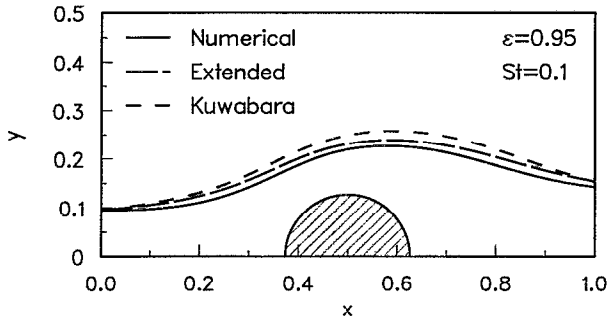


FIG. 10. Sample trajectories for the different solutions.

the particle size is comparable to the mean-free path of the fluid. The nondimensional form of Eq. (49) is

$$\mathrm{St}\frac{d\mathbf{u}_p}{dt}=(\mathbf{u}-\mathbf{u}_p), \tag{50}$$

where St is the Stokes number, defined by

$$\mathrm{St}=c_s\frac{2}{9}\frac{\rho_p^*\langle u^*\rangle R_p^{*2}}{\mu^* c^*}. \tag{51}$$

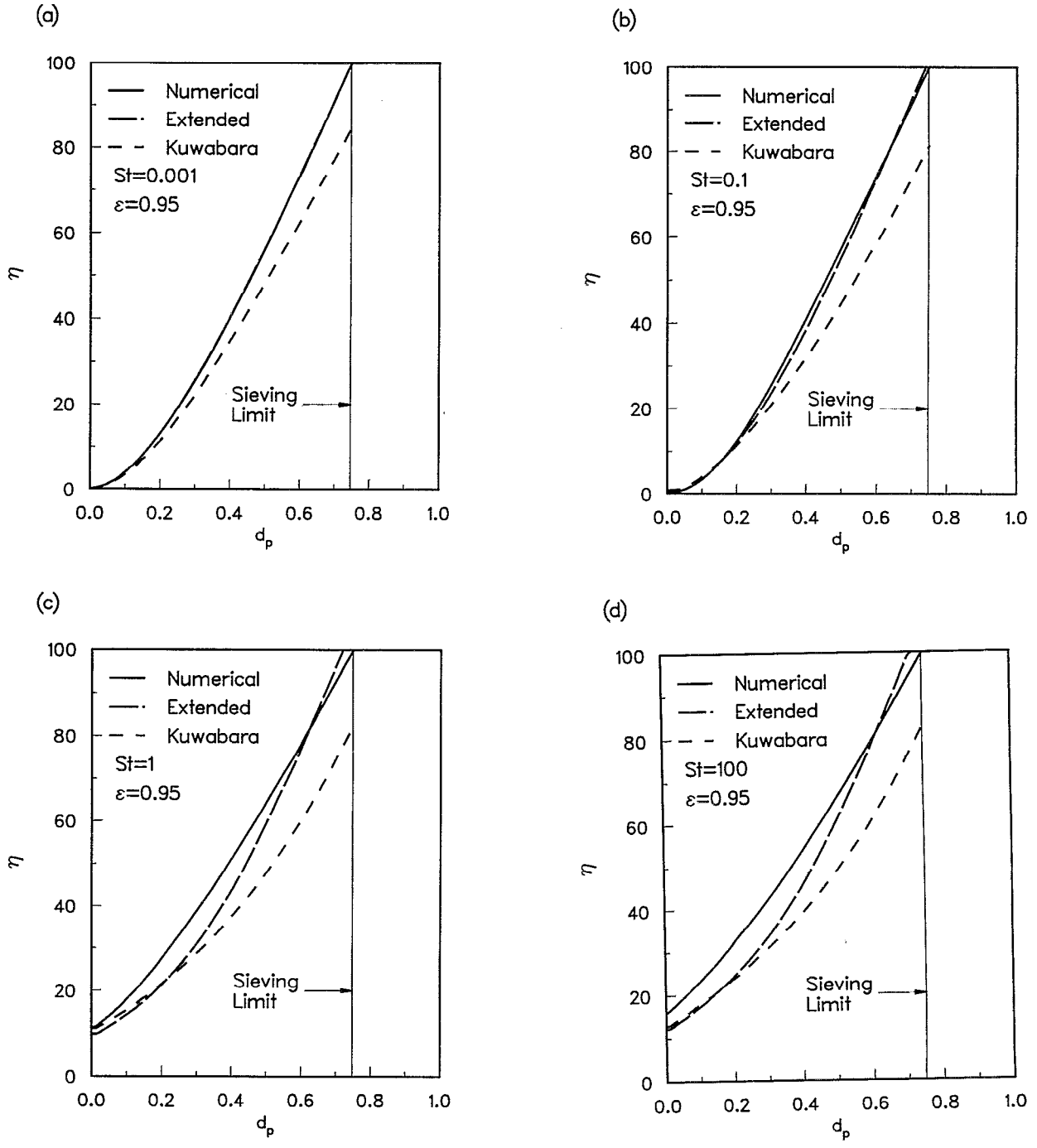


FIG. 11. Particle collection efficiencies for $\epsilon=0.95$ and (a) St=0.001, (b) St=0.1, (c) St=1, and (d) St=100.

The particle velocity vector $\mathbf{u}_p$ is found by numerical integration of Eq. (50). The explicit scheme is used for the integration. The fluid velocity vector $\mathbf{u}$ is obtained from the different solutions (numerical, extended analytic, and Kuwabara).

### A. Periodic flow regime

For high Stokes numbers, the fluid flow has less influence on the particle trajectory and particle inertial effect dominates. For low Stokes numbers, the fluid flow dominates the particle trajectory. Thus the previous section on impaction is the limit for the small Stokes numbers. Figure 10 shows some sample trajectories for St=0.1 using the different solutions methods. The extended analytic solution predicts better the particle trajectories than the Kuwabara solution and both are compared with the numerical solution.

In Fig. 11 we examine the particle collection efficiency for the Kuwabara, the extended, and the numerical solutions. Results are shown for four Stokes numbers that are representative of the full range of Stokes numbers. As in the previous section, we have assumed that the particles entering the unit cell are uniformly distributed in the fluid and have a local velocity equal to that of the fluid at the inlet boundary of the unit cell. The results of the previous section on the particle impaction agree well with the small Stokes number results in Fig. 11(a). Figure 11(b) shows that at St=0.1 a small deviation occurs in the predictions given by the numerical and the extended analytic solution. This deviation becomes larger as the Stokes number increases, as shown in Figs. 11(c) and 11(d). Also, as the Stokes number increases, the efficiency increases. In all cases the extended analytic solution gives a better prediction of the particle collection efficiency than does the Kuwabara solution. For small particle diameters and high Stokes number (i.e., St$\geqslant$1), the Kuwabara solution and the extended solutions underpredict the particle collection efficiency, as shown in Figs. 11(c) and 11(d). This is because the particle trajectories are strongly dependent on the initial conditions. Both the Kuwabara and the extended analytic solutions have a nonzero $v$ component of the velocity at the inlet of the unit cell. For the numerical solution, due to the assumed symmetry, this velocity is very small compared to the $u$ component. The nonzero $v$ component of velocity in the analytic solutions and for high Stokes numbers (i.e., St$>$10) makes the particle path oblique with respect to the $x$ axis of the unit cell. Hence the particle capture efficiency is lower than the numerical prediction. The effect of making the $v$ component of velocity zero at the inlet is shown in Fig. 12 for high Stokes numbers. The analytic solutions predict higher efficiency than the numerical solution. Note that for the numerical solution the trajectory of the particle is a straight line along the $x$ axis for high Stokes numbers, and therefore the particle efficiency can be predicted from the geometry consideration and inlet velocity.

In comparing the results given in Fig. 12, where the $y$ component of velocity is zero, to those in Figs. 11(c) and 11(d), where the $y$ component of velocity is nonzero, a

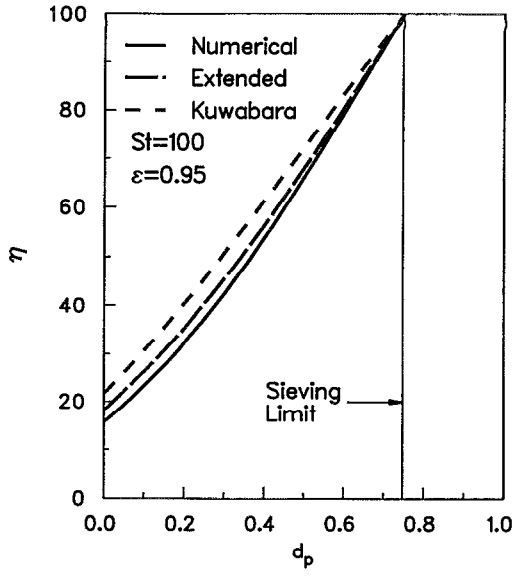


FIG. 12. Effects of initial conditions on particle collection efficiency using $v_p(-0.5,y)=0$ (St=100 and $\epsilon=0.95$).

care must be taken. A comparison between the prediction of the different methods (for the inertial impaction) can only be made for the high Stokes number asymptotes, with the same inlet velocity. In this limit, the fluid has no influence on the particle trajectory, so assuming the same initial velocity for the fluid and particle is not physically acceptable. Thus, the results given in Fig. 12 are more realistic and the results in Figs. 11(c) and 11(d) show how the initial values can effect the solution.

The collection efficiency is also examined for $\epsilon=0.8$, and the results are shown in Fig. 13. For small Stokes numbers [Fig. 13(a)], the efficiency predicted using the extended analytic solution is in excellent agreement with those predicted from the numerical solution. However, the efficiency predicted using the Kuwabara solution shows larger discrepancy than for the case of $\epsilon=0.95$, as shown in Figs. 11(a) and 11(b). This is because for $\epsilon=0.8$, the effect of the neighboring particles is more significant and the Kuwabara solution does not take that into account. For St=0.1, Fig. 13(b) shows that the inertial effects increase and the efficiency prediction of the extended analytic and the numerical solutions deviate. For St$\geqslant$1, the inertial effects become significant, and, as shown in Figs. 13(c) and 13(d), the deviations between the different predictions is more apparent. These deviations are more significant than those for $\epsilon=0.95$, shown in Figs. 11(c) and 11(d).

### B. Entrance flow regime

In addition to the accuracy that the numerical method presents over the analytic solutions, it is able to simulate flow in the entrance to the filter. In this region the condition of periodicity of the fluid flow does not apply. These numerical simulations show that for creeping flows the fluid flow becomes periodic beyond the first unit cell. The numerically obtained flow field is used to compute the par-

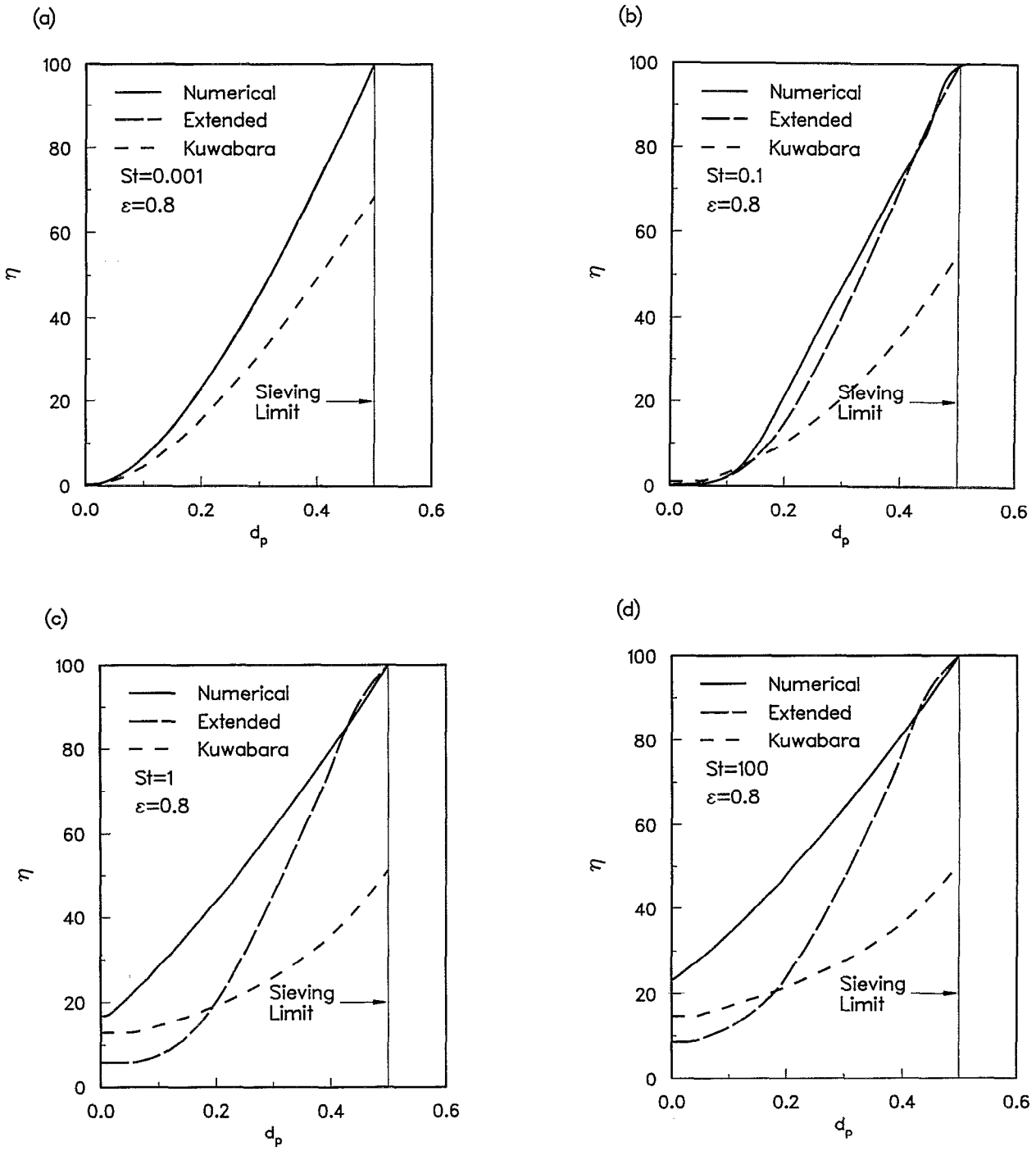


FIG. 13. Same as Fig. 11 for $\epsilon=0.8$.

ticle collection for low and high Stokes numbers. For low Stokes numbers, the efficiencies are very close to those predicted using the flow field solution for the periodic (i.e., bulk). For high Stokes numbers, Fig. 14 shows that the efficiencies for the entrance region and the bulk region are different, because the particle trajectory is influenced by the initial conditions. For small particle diameters, the numerical results for the entrance region predict efficiencies, which are closer to the analytic solutions. For large particles, the Kuwabara solution deviates, but the extended solution follows the same trend as the numerical results.

## VII. RECTIFICATION OF PARTICLE TRAJECTORIES

In the section on impaction, particles leaving one unit cell could not be collected in the next periodic cell unless some diffusion and/or a body force such as the gravity, an electrostatic, or the van der Waals force are added. Since

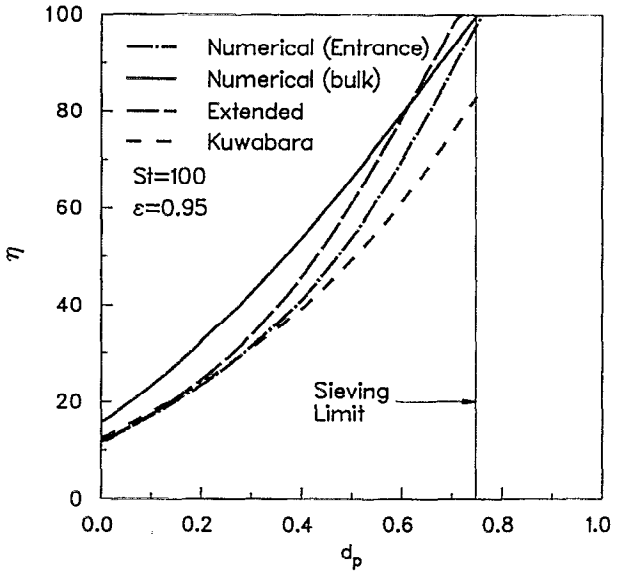


FIG. 14. Particle collection efficiency at the entrance region of the packed bed of cylinders compared to the extended analytic solution, Kuwabara and the numerical solution in bulk for St=100 ($\epsilon$=0.95).

the limiting streamlines are periodic, then for all following cells in a periodic structure all particles on the dividing streamline (i.e., capturing streamwise mentioned in Sec. V) barely miss collection on each downstream fiber past the first. The addition of an infinitesimal diffusion or a body force causes collection on these downstream fibers.

We propose that for the inertial impaction it may be possible for the in-line arrangement of fibers and downstream of the first fiber to have no collection of particles for a small but finite body force. To illustrate the phenomena, particle trajectory are given in Fig. 15 for the numerical, extended analytic, and the Kuwabara solution. After the first fiber is missed, the particle gradually, after passing through a number of unit cells (fibers), moves toward the center point between the fibers. All trajectories of the particles moving parallel to the flow and not collected at the first fiber display this behavior.

To explain this behavior consider the extended analytic solution. To simplify the problem we will assume a large Stokes number. Thus, to a first approximation, the trajectory is parallel to the $x$ axis. The fluid velocity in the Cartesian coordinates can be found from Eq. (38) by using the chain rule. To the first approximation, we assume that $y$ is nearly constant for large Stokes numbers and $v=0$ at the boundary. The nondimensional equation for the particle velocity is given by Eq. (50). To estimate the time it takes for the particle to transverse unit cell, we can note that the fluid flow is symmetric about $x=0$. Thus the amount $U$ retarded upstream, is accelerated by the fluid an equal amount downstream. This approximation is valid only as long as $y=$const is a reasonable approximation. Thus the time for crossing the unit cell is approximated by

$$t=\langle u\rangle_A/x, \tag{52}$$

where $\langle u\rangle_A$ is the area average velocity along the $x$ direction is given by

$$\langle u\rangle_A=\int_{-0.5}^{0.5} u(x,y)dx. \tag{53}$$

To a first approximation we can assume $dt=dx/\langle u\rangle_A$. By use of the integration factor $\exp(t/\mathrm{St})$, we can cast the $y$ component of the velocity as

$$e^{t_1/\mathrm{St}}v_{p_1}-v_{p_0}=\int_0^{t_1}\frac{v}{\mathrm{St}}e^{t/\mathrm{St}}\,dt. \tag{54}$$

Recasting the equation in $x$ rather than $t$, it becomes

$$v_{p_1}=\frac{e^{-x_1/(\langle u\rangle_A\mathrm{St})}}{\langle u\rangle_A}\int_0^{x_1/\langle u\rangle_A}\frac{v}{\mathrm{St}}e^{x/(\langle u\rangle_A\mathrm{St})}dx, \tag{55}$$

where we have substituted $t=x/\langle u\rangle_A$. We integrate once more to obtain an equation for $\delta y$, the displacement perpendicular to the $x$ axis a trajectory receives as it passes through a unit cell is

$$\delta y=y-y_0=\int_0^{1/(2\langle u\rangle_A)}\frac{e^{-x_1/(\langle u\rangle_A\mathrm{St})}}{\langle u\rangle_A}\times\int_0^{x_1/\langle u\rangle_A}\frac{v}{\mathrm{St}}e^{x/(\langle u\rangle_A\mathrm{St})}dx\,dx_1. \tag{56}$$

This formula can be analytically integrated using the extended analytic solution and a symbolic algebra package, such as MATHEMATICA. The resulting formula is unwieldy. However, by breaking up the integration into two sections, before and aft of the fiber, we can understand the effect analytically. From the above formula we can see that the positive $v$ component of velocity encountered before the cylinder displaces the near horizontal trajectory toward larger $y$ values. The $v$ velocities aft the fiber and in the opposite direction try to counteract the displacement that occurred upstream of the current fiber. The downstream fluid $v$ component of velocity are not able to counteract the full $y$ displacements resulting from the fluid upstream of the fiber. The reason that the positive $\delta y$ displacement occurring upstream of the fiber moves the trajectory up a bit and as it enters the downstream side the particle see smaller velocities because the particle is farther from the fiber. Thus in each unit cell the particle receives a net displacement toward the centerline between cylinders. Then there is a "rectification" of the particle displacement

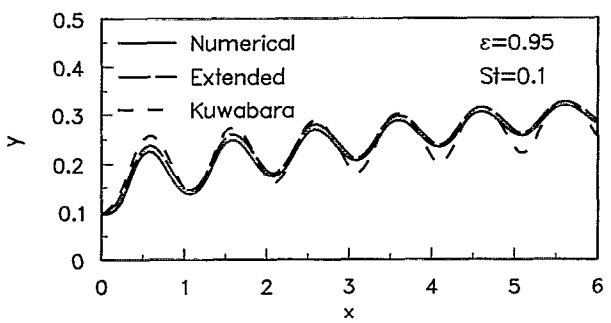


FIG. 15. Particle displacement after crossing multiple cells.

TABLE II. Rectification of the particles trajectories crossing many cells shown by the vertical displacement of the particle at the boundary of each cell (St=0.1 and $\epsilon$=0.95).

| | Numerical integration | | |
|---|---|---|---|
| Cell | Numerical velocity field | Extended velocity field | Analytic integration |
| 0 | 0.095 | 0.095 | 0.095 |
| 1 | 0.140 | 0.151 | 0.156 |
| 2 | 0.178 | 0.187 | 0.194 |
| 3 | 0.211 | 0.218 | 0.226 |
| 4 | 0.239 | 0.245 | 0.255 |
| 5 | 0.262 | 0.268 | 0.274 |
| 6 | 0.281 | 0.287 | 0.289 |

from the fluid flow. This effect occurs for any finite Stokes numbers. The Stokes number just determines how quickly this rectification occurs and over what number of cells it takes place. The final result is that after passing enough fibers, particles move to the centerline between the fibers.

In other words, by integrating the velocity to obtain the small $y$ displacement, we show that $dy$ upstream of a fiber is positive and always greater than the smaller negative $dy$ aft of the fiber. Since $dy$ starts the downstream trajectory farther from the fiber, the $v$ component of velocities are less and the particle does not move to the original $y$ value. For large Stokes numbers, this $dy$ is small, but accumulates for each fiber that is passed. The net effect is a rectification and after many cells the particle is moved away from the fiber, and the possibility of collection is reduced, even if small forces are included. Some sample $\delta y$ values are presented in Table II for different Stokes numbers and the different fluid flow solutions. The displacement values are obtained using the analytical approach given by Eq. (56) and the numerical integration of Eq. (50) using the numerical and extended analytic solutions. The results given in Table II show good agreement between the different methods. This rectification process can be generalized for the in-line arrangement of fibers, beyond the doubly periodic arrangement considered here. This effect can be used to align particles.

## VIII. CONCLUSIONS

The Kuwabara solution for flow through an in-line arrangement of cylinders has been extended, and a compact extended solution is found. The extended analytic solution improves prediction for the efficiency of particle collection by fibrous filters. The advantage of this improved analytic solution is that it can be used for further analytic investigations of fluid flow in fibrous filters without undo complexity. The formula for the streamfunction is given by Eq. (38).

We calculate the analytic efficiencies for particle collection by impaction and show that the results agree well with the numerical simulations. We also investigate anisotropic arrangements of cylinders. The formulas for the streamfunction are given by Eqs. (44) and (45) using two porosities $\epsilon$=0.95 and 0.8, respectively.

The "trajectory rectification," where the particles are less likely to be collected, as they are moved away from the fiber by the fluid flow, is also discussed. A small body force would not alter this conclusion, because no collection past the first cell would occur beyond the first cell. However, a body force greater than a critical value determined by the Stokes number can alter this. Thus, only diffusion and body forces larger than a critical magnitude would cause collection of particles beyond the first unit cell in the fiber lattice. In the case of negligible diffusion and body force, the fluid flow through these periodic structures can be used to align particles.

## ACKNOWLEDGMENT

We would like to thank Dr. Werner Bergman of the Lawrence Livermore National Laboratory for his financial and technical support of this project.

[1] S. Kuwabara, "The Forces experienced by randomly distributed parallel circular cylinders or spheres in a viscous flow at small Reynolds numbers," J. Phys. Soc. Jpn. **14**, 727 (1959).
[2] D. O. Banks, "Stokes flow through a system of parallel infinite cylinders with axes oriented at an angle to the direction of mean flow," Part. Sci. Technol. **5**, 339 (1987).
[3] D. O. Banks, and G. J. Kurowski, "Inertial efficiency of cylindrical collectors at an angle to the mean flow direction of flow," Aerosol Sci. Technol. **12**, 312 (1990).
[4] C.-u. Choo and C. Tien, "Hydrosol deposition in fibrous beds," Sep. Technol. **1**, 122 (1991).
[5] A. S. Sangani and A. Acrivos, "Slow flow past periodic arrays with application to heat transfer," Int. J. Multiphase Flow **81**, 193 (1982).
[6] M. Sahraoui and M. Kaviany, "Slip and no-slip velocity boundary conditions at interface of porous, plain media," Int. J. Heat Mass Transfer **35**, 927 (1992).
[7] H. T. Prata and E. M. Sparrow, "Forced convection evaporation from a cavity containing a liquid whose surface is curved by capillarity: Computations in interlocking rectangular and cylindrical domains," Num. Heat Transfer **12**, 667 (1985).
[8] S. V. Patankar, *Numerical Heat Transfer and Fluid Flow* (Hemisphere, Washington, DC, 1980).
[9] M. Kaviany, *Principles of Heat Transfer in Porous Media* (Springer-Verlag, New York, 1991), p. 104.
[10] B. Y. H. Liu and K. L. Rubow, "Air filtration by fibrous filters," *Fluid Filtration: Gas*, ASTM STP 975 (ASTM, Philadelphia, PA, 1986), Vol. 1.
[11] H. Hasimoto, "On the periodic fundamental solution of the Stokes equation and their application to viscous flow past a cubic array of spheres," J. Fluid Mech. **5**, 317 (1959).
[12] C. Tien, *Granular Filtration of Aerosols and Hydrosols* (Butterworth, Stoneham, MA, 1989).